CHEMISTRY OF MATERIALS

ARTICLE

pubs.acs.org/cm

Mechanistic Processes Underlying Biomimetic Synthesis of Silica Nanotubes from Self-Assembled Ultrashort Peptide Templates

Shengjie Wang,[†] Xin Ge,[†] Junyi Xue,[†] Haiming Fan,[†] Linjia Mu,[†] Yanpeng Li,[†] Hai Xu,[*,†] and Jian R. Lu[*,‡]

[†]State Key Laboratory of Heavy Oil Processing and the Center for Bioengineering and Biotechnology, China University of Petroleum (East China), Qingdao 266555, People's Republic of China

[‡]Biological Physics Group, School of Physics and Astronomy, University of Manchester, Schuster Building, Manchester M139JP, United Kingdom

Supporting Information

ABSTRACT: This work reports a mechanistic study of template-directed synthesis of silica nanomaterials utilizing self-assembled peptide nanotubes as scaffolds. An ultrashort amphiphilic peptide (I_3K) underwent self-assembly in aqueous solution under ambient conditions to form long and uniform nanotubes. The assembled peptide nanotubes then were used as templates for the subsequent fabrication of silica nanotubes from tetraethoxysilane (TEOS), also under ambient conditions. In order to gain better insight into the mediation of peptide self-assembly on the formation of silica nanostructures, we have carefully investigated environmental influences including the concentrations of peptide and silica precursor, solution pH, and reaction time, with the full screening of the processes by TEM, SEM, ^{29}Si MAS NMR, FTIR, and TG-MS. The results revealed that, while peptide nanotubes worked as scaffolds for the formation of tubular silica structures, the surfaces of these peptide nanotubes served as catalytic sites for both hydrolysis and condensation of TEOS, thereby working as templates for directing silica deposition. Because the electrostatic attraction of the negatively charged silica intermediates onto the positively charged surface of peptide nanotubes drove the templating process, tuning of such an interaction by adjusting the solution conditions (such as pH) affected silica morphological structures. Silica tended to deposit along the exterior surface of the template at undersaturation over weak acidic and neutral pH ranges, while silica intermediates overcame diffusion resistance and moved inside the tubular template over mild basic pH ranges, enabling silica precipitation along the interior surface. This work has thus demonstrated that the morphological nanostructures of silica can be controlled by adjusting the silicification conditions (such as peptide concentration and solution pH) under an ambient environment, thus avoiding harsh chemicals or extreme reaction conditions.

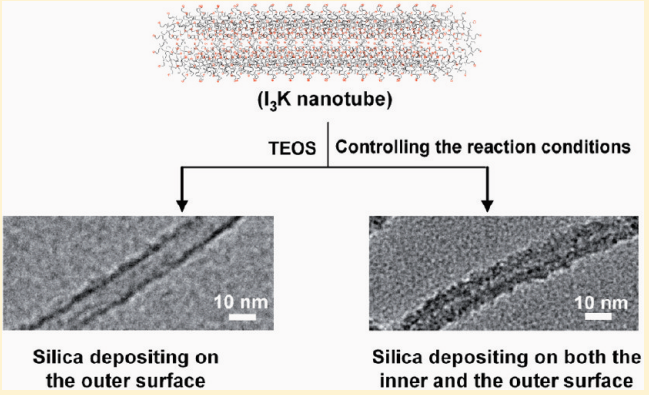

KEYWORDS: silica nanotubes, peptide nanotubes, peptide templates, biomimetic silicification, I_3K, peptide amphiphiles, silica nanostructures, biomimetic synthesis

1. INTRODUCTION

Silica-based nanomaterials have been extensively investigated for many years, because of their potential applications in a diverse range of technologies including catalysis, sensing, separation, enzyme immobilization, and gene and drug delivery.[1−5] Conventional manufacturing processes of silica nanomaterials usually require severe conditions such as high temperature and high pressure, extreme pH, and extensive use of deleterious reagents and solvents. In addition, these chemically based fabrications usually possess relatively limited controls over the morphology and structure of the resulting silica nanomaterials, which are often accompanied by problematic byproduct.[1,6−8] In contrast, many living organisms (particularly small aquatic species, such as diatoms and sponges) produce copious silica nanomaterials constituting most of their body masses under benign reaction conditions (i.e., ambient temperature and pressure and neutral pH). These siliceous materials incorporate intricately patterned nanostructures and remarkable properties such as mechanical strength and light conduction.[9−14] Importantly, these intriguing nanostructures are highly species-specific and organisms have great spatial and temporal controls over their formation.[15,16] At present, biogenic silica nanomaterials are superior to most existing man-made versions in formation process, structure, and property. Thus, understanding the mechanistic processes underlying biogenic synthesis is a crucial step that will offer a paradigm for better control of nanosilica production.

Considerable progress has been made over the past decade in the understanding of molecular mechanisms underpinning biosilicification and the biomimetic synthesis of patterned nanosilica. Although the genetic basis for organisms harnessing nanosilica

Received: February 7, 2011
Revised: March 31, 2011
Published: April 14, 2011

deposition and patterning still remains poorly understood, it is currently known that organic molecules such as polyamines, silaffins, and silicateins are intimately associated with the biogenesis of silica.[12,17−20] They have been proposed to play multiple roles during the *in vivo* formation of silica nanomaterials, by serving as catalysts, templates, and scaffolds.[12,18,21,22] After being extracted from organisms, these biomolecules have been shown to undertake the *in vitro* catalysis of the polycondensation of different silica precursors (i.e., silicic acid and silicon alkoxides) and precipitate silica from aqueous solution under circum-neutral pH. For the biomimetic synthesis of materials, however, the direct use of bioextracts has several drawbacks.[14] Isolation and purification of biomolecules from organisms are generally laborious and costly. Importantly, their secondary structural conformations and specific characteristics (i.e., self-assembling) that are most likely to be prerequisites for the formation of structured nanosilica may become lost during the extraction process. Biosilica containing biomasses are usually treated with strong acids such as HF for liberating biomolecules. Thus, the *in vitro* biosilicification with bioextracts often fails to produce hierarchical structures—a hallmark of biogenic silica, thereby limiting their potential applications. To circumvent these problems, numerous synthetic analogues that are commercially available have been exploited under relatively benign conditions, including short- and long-chain polyamines (i.e., tripropylenetetramine, pentapropylenehexamine, spermine, spermidine, polyallylamine, and polyethyleneimine),[23−27] poly(amino acids) (i.e., polylysine, polyhistidine, and polyarginine),[8,22,28,29] block copolymers (i.e., $PDPA_{23}$-$PDMA_{68}$, cysteine-lysine and lysine-phenylalanine block copolypeptides),[27,30,31] and peptides (i.e., SAF peptides, Lanreotide, P_{11}-3 peptide, and lipopeptides).[32−35] These synthetic analogues mimic the composition and sequence characteristics of bioextracts and are generally cationic and rich in amine groups and basic amino acids such as lysine, histidine, and arginine. Among them, chemicals with specific conformations and well-defined assembling structures are particularly attractive, because they allow us to undertake *in vitro* fabrication of silica nanostructures with better morphological control. For instance, many *de novo* designed peptides adopt α-helical or β-sheet conformations and are able to self-assemble into nanofibrils in aqueous solution, with positively charged moieties on their surfaces. These peptide-based nanostructures are subsequently applied as templates to direct silica deposition from its precursors (i.e., silicic acid and TEOS) in aqueous solution at neutral pH, eventually leading to the formation of well-defined silica nanotubes.[32,35] These studies present an exciting list of examples for the biomimetic synthesis of hierarchical nanostructures from bottom-up under benign environment, particularly considering the multiplicity of morphologies and functions available with engineered peptides. The template-direct synthesis strategy is clearly of great potential for the technological applications, because of its simplicity and high throughput.

In many of our previous studies, we have designed and synthesized a series of short amphiphilic peptides and revealed that they could undergo self-assembly at the interface and in aqueous solution to form various nanostructures with high stability.[36−43] Interestingly, ultrashort peptides such as I_3K formed long nanotubes that were sufficiently stable for templating the sol−gel condensation of TEOS at circum-neutral pH, yielding long silica nanotubes after removing the peptide substrate via calcination.[36] To the best of our knowledge, I_3K is the shortest amphiphilic self-assembling peptide utilized for templating nanostructured silica. It is of huge potential for practical applications, because it is easier to produce in a commercial scale. A crucial step toward realizing this ambition is to understand the key factors affecting these silica nanomaterials. Here, we report a systematic evaluation of the biomimetic synthesis of hybrid silica with controllable nanostructures via tuning environmental influences. We show that the morphology and nanostructures of silica nanomaterials can be easily regulated by changing the ratio of peptide to silica precursor, the solution pH, and the aging periods. Because these reactions and processes occurred under ambient conditions, the study has not only improved our understanding of peptide template-direct synthesis of biological silica formation, but also brought this process closer to practical applications.

2. EXPERIMENTAL SECTION

2.1. Chemicals and Materials. Protected amino acids (Fmoc-L-Ile-OH, Fmoc-L-Lys(Boc)−OH), Rink amide-MBHA resin, *O*-(1H-benzotriazole-1-yl)-*N*,*N*,*N*′,*N*′-tetramethyluronium hexafluorophosphate (HBTU), *N*-hydroxybenzotriazole anhydrous (HOBt), N,*N*′-diisopropyl ethylamine (DIEA), trifluoroacetic acid (TFA), piperidine, and triisopropylsilane (TIS) were purchased from GL Biochem. (Shanghai) Ltd. Dichloromethane (DCM) and dimethylformamide (DMF) were obtained from Sinopharm Chemical Reagent Co. Ltd., and redistilled and dried with molecular sieves before use. Tetraethoxysilane (TEOS), anhydrous ethanol, diethyl ether, and other reagents were purchased from Sigma−Aldrich and used as received. All water used was obtained from a Millipore water purification system with a minimum resistivity of 18.0 MΩ cm.

2.2. Peptide Synthesis. I_3K was synthesized by standard Fmoc solid-phase synthesis on a CEM Liberty microwave peptide synthesizer, in which the C-terminus was amidated and the N-terminus was acetylated to limit the charge on the peptide purely arising from the lysine residue side chain. The detailed procedures were similar to those described in our previous work.[36,37] The crude product was purified by deposition with copious cold ether at least six times, to achieve a high purity of >98%, as indicated by reverse-phase high-performance liquid chromatography (HPLC) and matrix-assisted laser desorption ionization-time of flight (MALDI-TOF) mass spectroscopy (MS) characterizations (see Figures S1 and S2 in the Supporting Information).

2.3. Preparation of I_3K Solution. The purified I_3K displayed excellent solubility in aqueous solution. Here, the stock solution was created at 4 mM, with a solution of pH ∼7. The peptide solution was aged at ambient temperature for at least one week and then used for characterization and silica synthesis.

2.4. Silica Synthesis. Silica formation was achieved by directing the sol−gel reaction of TEOS with I_3K nanotubes at room temperature. To gain insight into the mechanistic role of I_3K during this biomimetic synthesis, the effects of concentration, pH, and reaction time were investigated in detail. In a typical experiment, TEOS was dissolved into a certain volume of ethanol and then mixed with an equal volume of mature I_3K solution. The pH of mixed solution was slightly adjusted to desired values and incubated at 20 ± 1 °C and atmospheric pressure in a static environment for different times. Note that, for a specific analysis, periodic sample collection was performed during the incubation process. Finally, the precipitate was collected by centrifugation at 30 000 rpm for 30 min. The resulting gel-like precipitate was freeze-dried to generate loose powder. After washing alternately with ethanol and water at least four times, the powder was freeze-dried again. Part of the powder was characterized directly as silica hybrids, and the rest was calcined at 550 °C for 8 h in air to remove organic templates and generate silica nanostructures.

2.5. Instrumental Characterizations. To characterize the structural conformation and morphology of I_3K assembly, circular dichroism (CD) and transmission electron microscopy (TEM) measurements were performed. The CD spectra were recorded on a MOS-450 spectrometer (Biologic, France) at 25 °C with a 1-mm quartz cell, and expressed as $[\theta]$ (deg cm^2 $dmol^{-1}$) versus wavelength. TEM imaging was performed on a JEOL-2100UHR electron microscope operated at

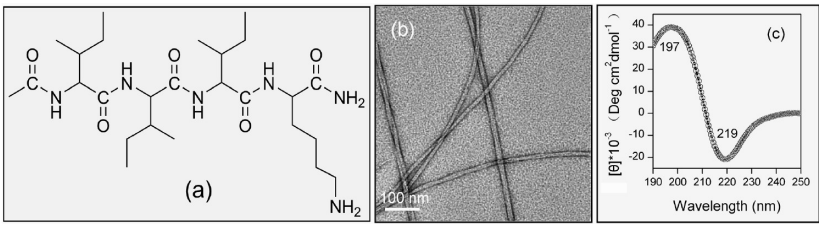

Figure 1. (a) Chemical structure of I_3K; (b) negative-stain TEM micrograph of I_3K at 4 mM, showing a nanotubular structure; and (3) the corresponding CD spectrum of I_3K at 4 mM in aqueous solution.

200 kV after the peptide samples were negatively stained with 2% uranyl acetate. More experimental details with respect to these analyses have been given in our previous studies.[36,37]

Silica and hybrid silica samples were characterized with TEM and scanning electron microscopy (SEM) to reveal their structural and morphological information. TEM measurements were also performed on a JEOL-2100UHR electron microscope operated at 200 kV. Note that the samples were dispersed in ethanol and directly pipetted on to the TEM grid for subsequent characterization, and no staining agent was applied. SEM imaging was conducted using a JEOL S-480 field emission SEM (FE-SEM) microscope with an acceleration voltage of 3.0 kV. The SEM samples were prepared by placing a droplet of a suspension of silica or hybrid silica powder in ethanol on an aluminum stub and allowing the ethanol to evaporate.

The degree of polycondensation of the silica framework (Q4, Q3, and Q2) within hybrid silica samples was assessed by ^{29}Si MAS NMR spectra recorded on a Bruker Avance III 400 MHz NMR spectrometer at 20 °C. The relaxation delay for these measurements was 5 s, and the resonance frequency was 79.5 MHz. Date were processed using Origin 8.0 software and least-squares-fitted to Lorentz lineshapes.

Thermogravimetric (TG) measurements were carried out on a TG (STA 449C)/MS (QMS 403C) instrument (Netzsch, Germany) equipped with a heat flow detector. The hybrid silica samples were heated at a rate of 20 °C min^{-1} from 30 °C to 800 °C in air, to ensure complete combustion of all organic components. Changes of mass and heat flow during the heating process were recorded. The gas released was collected and analyzed via a mass spectrometer.

Infrared spectroscopy measurements were conducted on a Nicolet 6700 FT-IR spectrometer, using thin KBr as the sample holder. The resolution in the spectrum collection was set at 4 cm^{-1}, and the scanning range was set from 4000 cm^{-1} to 400 cm^{-1}.

3. RESULTS

3.1. Peptide Self-Assembly. The chemical structure of I_3K is shown in Figure 1a. Its amphiphilic nature and intermolecular hydrogen bonding endow a strong self-assembling ability in aqueous solution. The TEM micrograph in Figure 1b shows that I_3K aggregates formed at 4 mM exhibit tubular structural features with uniform diameter. The length of the tubes reaches a few micrometers, and the outer and inner diameters of I_3K nanotubes have been determined to be ~10 nm and ~5 nm, respectively, with the help of SANS technique.[36] As shown in Figure 1c, the CD spectrum of the 4 mM I_3K solution displays a positive maximum at 197 nm and a negative minimum at 219 nm, indicating that the peptide is self-assembled in a β-sheet conformation. Note that the above structural features of I_3K assemblies are constant over a wide pH range of 3−9. In addition, the mature I_3K nanotubes are extremely stable, with respect to dilution, temperature below 90 °C, and organic solvents (including ethanol, acetonitrile, and acetone).[36]

3.2. Templating for Silica Nanotube Formation. TEOS is usually difficult to hydrolyze and condense in aqueous solution without a catalyst at circum-neutral pH. The control experiments in the absence of any additive showed no precipitation, even when left for a month. In contrast, upon mixing with an equal volume of a 4 mM I_3K solution at pH 7 (the I_3K concentration in the reacting mixture was therefore reduced to 2 mM and similarly hereinafter, unless otherwise noted), it underwent the sol−gel reaction. The TEM image of collected precipitates (after aging for 4 days, before calcination) indicates that silica preferentially deposits around the surface of I_3K nanotubes (see Figure 2a). However, when a peptide solution of 0.05 mM (lower than the I_3K critical aggregation concentration (CAC) of 0.45 mM) was applied without changing other silicification conditions, only nonspecific silica precipitates were obtained (see Figure 2b).

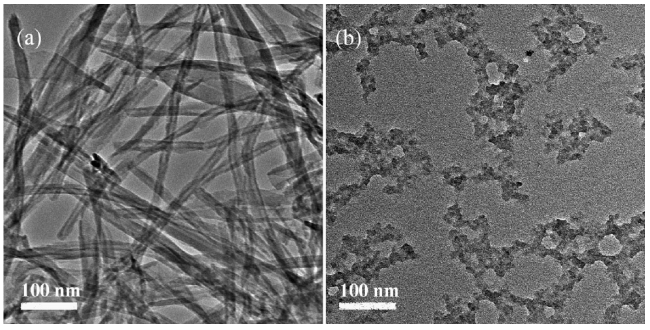

Figure 2. TEM images of (a) hybrid silica aggregates (i.e., peptide-silica composite) induced by I_3K nanotubes that were formed at 4 mM and (b) samples collected when a I_3K solution of 0.05 mM was applied. The TEOS concentration was 0.045 mM in both reacting mixtures, with the reaction time being 4 days at pH 7. Note that the critical aggregation concentration (CAC) of I_3K in aqueous solution was ~0.45 mM and that no defined aggregates were formed at 0.05 mM.

Figure 3a shows the Fourier transform infrared (FTIR) spectra of I_3K and the above tubular silica nanomaterials obtained before and after calcination. The hybrid silica (i.e., peptide−silica composite) displays three characteristic peaks of silica: −Si−O−Si− asymmetric stretching at 1089 cm^{-1}, symmetric stretching at 800 cm^{-1}, and −Si−OH stretching at 960 cm^{-1}. In addition, there are two further characteristic FTIR bands (cyan region in Figure 3a) at 1635 and 1543 cm^{-1}, arising from peptide amide I and II bands, respectively. The occurrence of the two characteristic peptide bands indicates the entrapment of I_3K nanotubes into silica precipitates through their templating. After calcination at 550 °C for 8 h, the characteristic bands of the peptide and Si−OH groups disappear as expected, suggesting that the peptide substrate can be removed and that the Si−OH groups are converted to Si−O−Si structures during the heating process. TG/DSC/MS measurements were also conducted with the above hybrid silica sample in air at a heating rate of 20 °C min^{-1}. As shown in Figure 3b, there is ~5% weight loss before

dx.doi.org/10.1021/cm2003885 |Chem. Mater. 2011, 23, 2466–2474

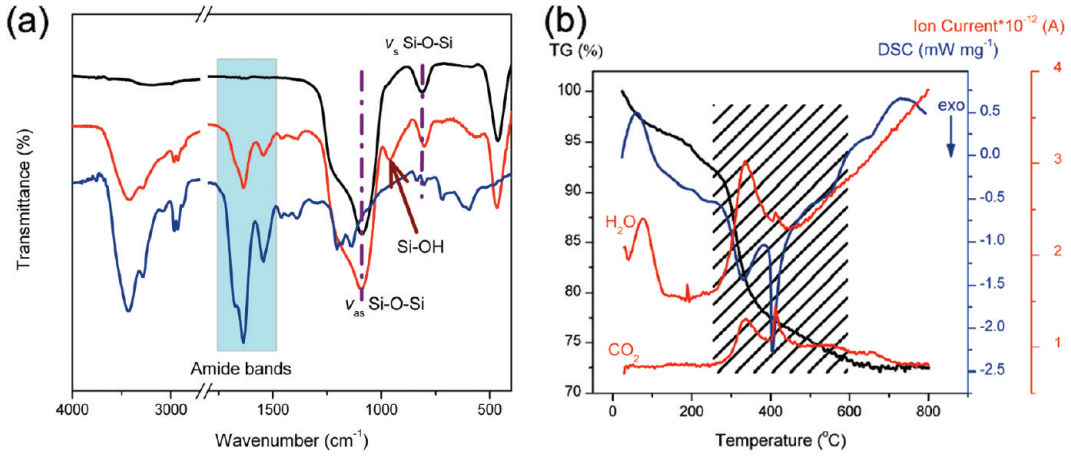

Figure 3. (a) FTIR spectra of I_3K (blue line) and I_3K templated silica before (red line) and after (black line) calcination at 550 °C for 8 h. (b) TG/DSC/MS curves for hybrid silica; the heating rate was set as 20 °C min^{-1} (color code: TG trace, black; DSC trace, blue; and MS trace, red). Note that the I_3K and TEOS concentrations in the reacting mixture were fixed as 2 and 0.045 mM, respectively, and the reaction proceeded for 4 days at pH 7.

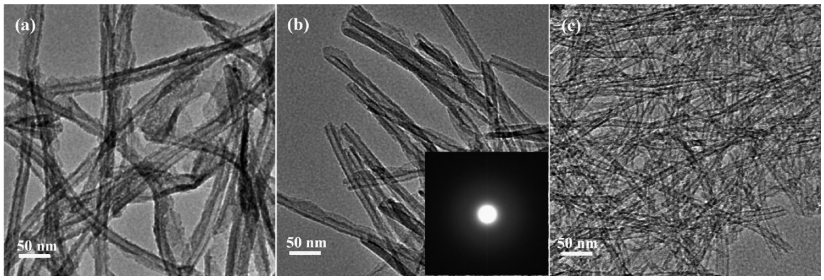

Figure 4. TEM images of calcined silica nanostructures prepared from different TEOS concentrations of (a) 0.225 mM, (b) 0.045 mM, and (c) 0.011 mM with a constant I_3K concentration of 2.0 mM. Aging was set for 4 days at pH 7 for the three samples. Inset in panel b shows the electron diffraction pattern in a selected area.

200 °C in the TG curve, which was attributed to the initial vaporization of superficial water. The main temperature region for weight loss occurs between 250 °C and 600 °C (shaded region in Figure 3b), where more than 20% of the mass loss was due to the combustion of organic materials, which can also be proved via the presence of MS signals for CO_2 and H_2O and exothermic peaks in the DSC curve in the same temperature range. This observation again indicates the entrapment of I_3K nanotubes into silica precipitates via templating.

3.3. Concentration. The templating capability of I_3K nanotubes for silica precipitation is affected by the ratio of I_3K to TEOS. Figure 4 shows TEM images of calcinated silica from various TEOS concentrations with a constant I_3K concentration of 2.0 mM. All of them exhibit tubular silica structures with an amorphous nature (see the selected-area electron diffraction (SAED) pattern inset in Figure 4b). The outer diameter seems to increase slightly, but more and more random precipitation occurs with increasing TEOS concentration. These results suggest that the nucleation of silica on I_3K nanotubes is preferred over bulk precipitation at relatively low supersaturation levels, while concentrations of TEOS above a certain value increase the level of nontemplated deposition associated with the hydrolysis/condensation reactions that are occurring in solution, as shown in Figure 4a. Thus, lower concentrations of TEOS favor the formation of regular silica nanotubes. As shown in Figure 4c, however, the template is coated with a thin silica layer if the concentration of TEOS is too low. As a result, only a small quantity of minerals can be obtained. Similar results were found in a silica synthesis mediated by a helix-based fibrous template.[32]

3.4. Influence of pH. To avoid having an acid or base become the primary catalyst, we investigated the pH effect around the neutral pH range (from 5 to 9), with a minimum amount of diluted HCl and NaOH solution to adjust the pH. Note that it is over such a pH range that the *in vivo* biosilicification typically occurs. In contrast, however, it is difficult to precipitate silica from TEOS *in vitro* over the same pH range in the absence of catalysts. Also note that the tubular structure of I_3K nanostructures remains constant over this pH range. Figure 5 shows the TEM images of calcined silica nanostructures prepared at different pH. At pH 5, although the tubular feature of silica precipitates exists, there is considerable nonspecific precipitation in the vicinity of the tubular network (see Figure 5a), suggesting weak template direction during the mineralizing process under the weak acidic condition. A subsequent increase to pH 7 leads to silica deposition mainly on the surface of the peptide templates with some nanotape-like structures (see Figure 5b). This observation indicates that the interaction between silicon species and the template improves as the pH increases. Interestingly, at pH 9, only tubular silica structures with uniform diameter are formed (Figure 5c), showing that there is a stronger mediation function by the peptide templates. The complementary SEM characterization of silica obtained at pH 9 confirms that homogeneous nanofibrous structures with a high length:diameter ratio are formed without any other irregular structures. (See Figure S3 in the Supporting Information.)

dx.doi.org/10.1021/cm2003885 |*Chem. Mater.* 2011, 23, 2466–2474

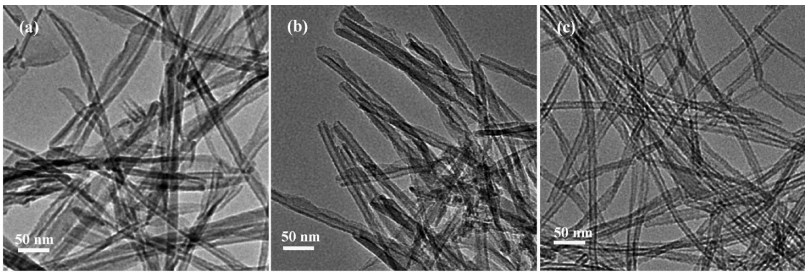

Figure 5. TEM images of calcined silica structures prepared at (a) pH 5, (b) pH 7, and (c) pH 9. Note that the I_3K and TEOS concentrations in the reacting mixture were fixed as 2 and 0.045 mM, respectively, and the reaction time was 4 days.

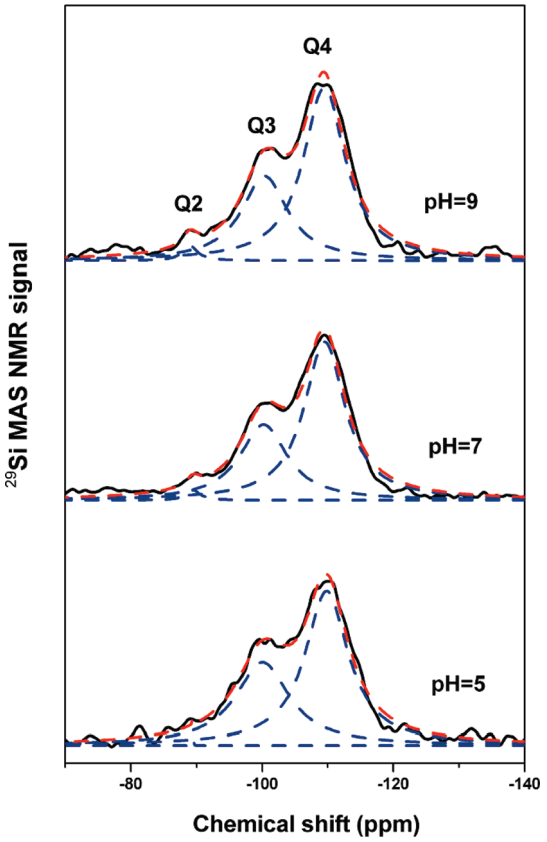

Figure 6. ^{29}Si MAS NMR spectra of silica hybrids after aging for 4 days at different pH. Note that the I_3K and TEOS concentrations in the reacting mixture were fixed as 2 and 0.045 mM, respectively. The experimental data (black lines) were processed using Origin 8.0 software and least-squares-fitted to Lorentz lineshapes. (Color code: black, experimental lines; blue, multipeak fitting lines; and red, sum of the blue lines.)

To evaluate the degree of polycondensation of the deposited silica at different pH, solid-state ^{29}Si MAS NMR measurements were performed with three silica hybrids prior to calcination. As shown in Figure 6, these silica nanostructures show two strong signals centered at −110 and −100 ppm, assigned to Q4 ($Si(OSi)_4$) and Q3 ($HOSi(OSi)_3$), respectively,[44,45] and the former is stronger than the latter. In addition, a very weak signal is observed at −90 ppm, attributed to Q2 ($(HO)_2Si(OSi)_2$). These observations suggest that the hybrid silica has a relatively high degree of polycondensation, demonstrating the excellent catalytic function of the I_3K template for the sol−gel reaction under these conditions. Relative changes in Q3 and Q4 species under

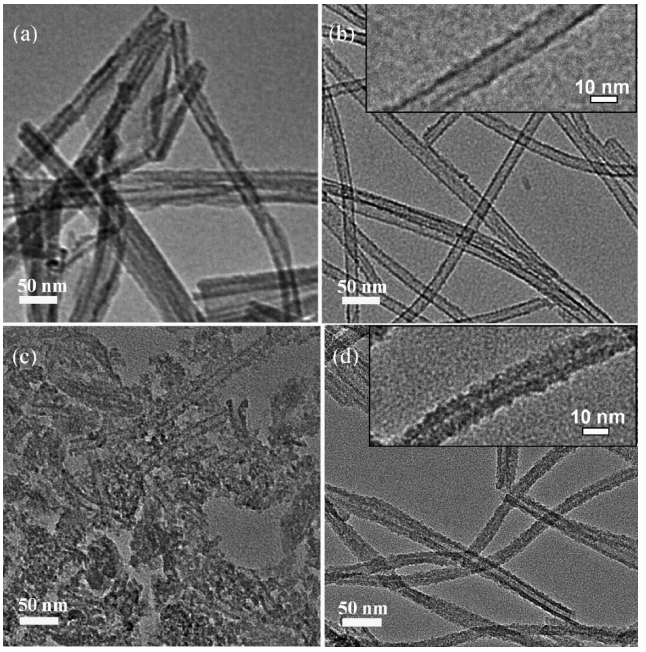

Figure 7. TEM images of calcined silica nanostructures after aging for 8 days at (a) pH 7 and (b) pH 9, and 16 days at (c) pH 7 and (d) pH 9. The insets in panels b and d show expanded images for 8 and 16 days at pH 9, respectively. The I_3K and TEOS concentrations in the reacting mixture were fixed as 2 and 0.045 mM, respectively.

different solution pH were analyzed by a curve-fitting procedure. The ratios of Q4 to Q3 were calculated as 1.49 (pH 5), 1.57 (pH 7) and 1.61 (pH 9), indicating a trend of increase of the degree of polycondensation for silica hybrids with increasing pH. However, the ratios of Q4 to Q3 changed in a narrow range, almost comparable to the experimental errors expected from the measurements. Given such experimental uncertainty, the slight increase in Q4/Q3 ratios shows a positive correlation with the trend of increase in the ionization of silica precursors with pH, indicating that increasing electrostatic attraction to the I_3K templates with rising pH favors a condensation reaction and consequent silica precipitation.[46]

3.5. Influence of Reaction Time. Compared with the TEM images aged for 4 days, the morphology of silica structures aged for 8 days showed no marked changes at pH 7 and pH 9 (see Figures 7a and 7b). However, when the reaction time was further extended to 16 days, the structural morphology changed noticeably. At pH 7, there was significant random silica deposition, together with silica nanotubes (Figure 7c), whereas there were

dx.doi.org/10.1021/cm2003885 |*Chem. Mater.* 2011, 23, 2466–2474

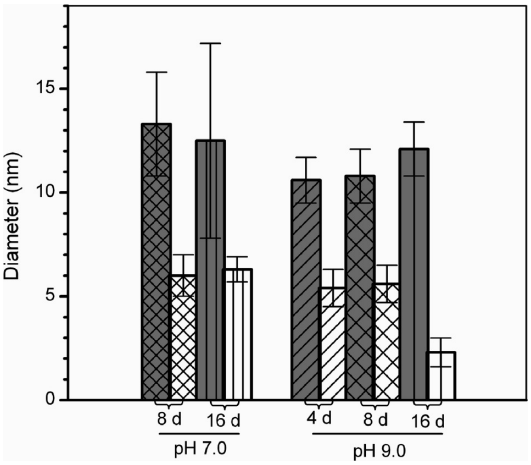

Figure 8. Diameters of silica nanotubes aging for different periods at different pH. The columns filled with gray and white represent the outer and inner diameters, respectively.

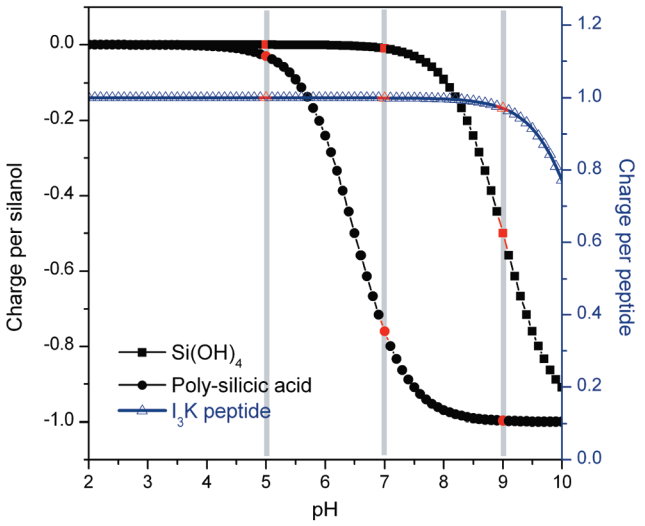

Figure 9. Influence of pH on the charge per silanol group for $Si(OH)_4$ and poly silicic acid (left axis) and per I_3K peptide (right axis).

only silica nanotubes at pH 9 (Figure 7d). To observe the dimensional changes more precisely, the diameters of silica nanotubes were measured for 120 samples, as shown in Figure 8. Both the outer and inner diameters (~13 nm and ~6 nm) at pH 7 showed no obvious changes with increased aging time until a point was reached where significant nondirected deposition occurred. Note that the outer diameters have a wide distribution for the samples obtained at pH 7, because of there being more than one type of structure and random aggregation on the exterior surface of the nanotubes. By contrast, for the sample obtained at pH 9, the inner diameters remain constant for 8 days and decrease considerably from 5.4 nm to 2.3 nm after aging for 16 days, whereas there is only a slight increase in the outer diameters during this period.

4. DISCUSSION

Lysine is especially abundant in diatom silica precipitating proteins (silaffins) and is thought to play a crucial role during the *in vivo* biosilicification. Many lysine-containing peptides and polypeptides have been successfully utilized for the biomimetic synthesis of silica. In our case of pH ≤9, the side-chain amine of lysine residue is protonated and I_3K molecules carry positive charges. Upon their assembly in aqueous solution, the cationic residues are distributed on the surface of the assembled nanostructures and exposed to the water environment. As expected, the sol−gel reaction of TEOS proceeded well in the presence of I_3K and silica deposition preferentially occurred around the surface of I_3K nanotubes. In contrast, random silica precipitates instead of templated structures were observed when the solution peptide concentration far below its CAC was applied. These observations imply different roles of I_3K nanotubes, that is, working as not only a catalyst for both the hydrolysis and condensation of TEOS but also as a template for directing silica deposition.

The sol−gel reaction of TEOS involves two steps, i.e., hydrolysis and condensation. Its hydrolysis allows the $-OC_2H_5$ groups being replaced by the −OH groups to produce silicic acid and/or partially hydrolyzed TEOS. They subsequently undergo the condensation reaction to form siloxane (Si−O−Si) linkages. Under the catalysis of I_3K, TEOS undergoes hydrolysis and condensation reactions to eventually produce rather highly polymerized silica, as is evident from the ^{29}Si MAS NMR spectra (Figure 6).

The driving force for the templating originated from the electrostatic attraction between the negatively charged silica intermediates and the positively charged surface of I_3K nanotubes. The silanol groups (Si−OH) of silica intermediates are liable to deprotonate, depending on environmental pH. The pK_a of the silanol groups decreases with the condensation state of intermediates; for instance, from ~9 for $Si(OH)_4$ to ~6.5 for polysilicic acids and hydrated silica.[1] For I_3K, the side-chain amine of its lysine residue is readily protonated in aqueous solution and its pK_a is close to 10.5. The calculated evolution of the charge with pH is shown in Figure 9 for silicic acid, polysilicic acids, and I_3K, using the Henderson−Hasselbach equation. Note that the pK_a of polysilicic acids was assumed to be 6.5, with no regard for their degree of polymerization. It is evident that the peptide is almost 100% protonated in the pH range of 5−9, but the charges of silica precursors change substantially from pH 5 to pH 9. At pH 5, silicic acid and polysilicic acids carry little negative charge (Figure 9). In this case, there was thus considerable random silica precipitation, because of the relative weak electrostatic attraction between silica intermediates and the peptide template. Because the surface lysine residues provide most of the catalytic sites for the sol−gel reaction, most nonspecific silica precipitates were still close to the tubular template. At pH 7, most polysilicic acids are negatively charged and the templating effect is, consequently, augmented, resulting in remarkable tubular silica structures. Furthermore, the templating effect of I_3K nanotubes at pH 7 could be easily mediated by varying the ratio of TEOS to peptide and the reaction time. For instance, reducing the ratio led to the formation of well-ordered silica nanotubes with little random precipitates (Figure 4c), because the intermediates produced in this case were limited, in comparison with positive charges on the template surface, resulting in well-ordered anchoring on the template surface. In contrast, increase in the ratio increased the degree of random silica precipitation (Figure 4a). Once the positive charges on the template surface were completely neutralized or embedded by the adsorbed silica anions with increasing silicification time, further increases in time led to the formation of random silica precipitates (see Figure 7c).

dx.doi.org/10.1021/cm2003885 |*Chem. Mater.* 2011, 23, 2466–2474

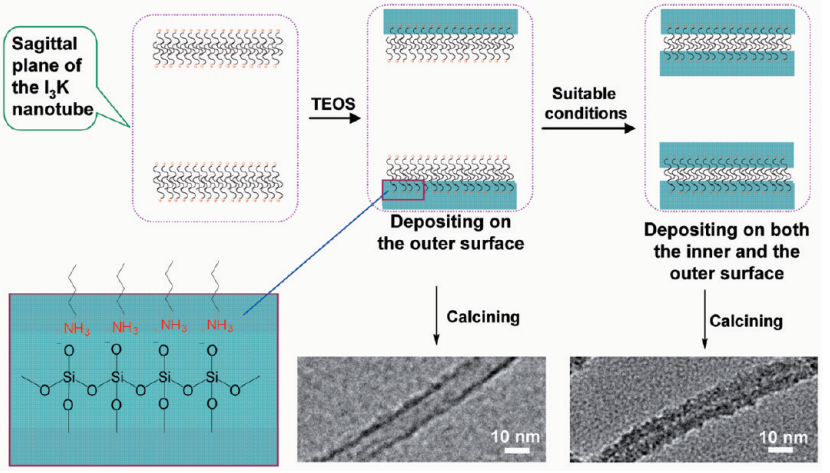

Figure 10. Schematic illustration of templating silica nanostructures by I_3K self-assembly.

At pH 9, the degree of deprotonation of silica intermediate species is further enhanced. As a result, strong electrostatic attraction with the I_3K nanotubes occurred and the templating effect became prominent, with only well-ordered silica nanotubes being formed. As a result of this strong attraction, further increases in reaction time to 16 days did not lead to the formation of random silica; instead, additional silica nucleation occurred along the inner surface of I_3K nanotubes, showing that, given sufficient driving force for templating, well-ordered silica nanomaterials were always preferred to the random precipitates.

From SANS studies, we have determined the outer and inner diameters of I_3K nanotubes to be ~10 nm and ~5 nm respectively, with a shell thickness of ~2.5 nm.[36] At pH 7, the outer and inner diameters of the resulting silica nanotubes are ~13 nm and ~6 nm, respectively, with a coating thickness of ~3.5 nm. These parameters can slightly vary as the reaction time increases from 8 days to 16 days. Depositing silica along the inner surface of narrow peptide nanotubes generally is difficult, because of the diffusion-limited transport of reactant and intermediate species.[33] Pouget et al. observed a symmetrical silica coating along the inner and outer surface of lanreotide nanotubes, which was due to the simultaneous occurrence of nanotube template reassembly and silica mineralization, in which both the inner and outer surfaces are equivalently accessible for silica reactants.[33] In our case, however, the I_3K nanotubes are unlikely to dissociate, because of their exceptional stability. Thus, we propose that a silica coating occurred only along the outer surface of the peptide nanotubes at pH 7.

Although there was slight variation with the outer diameter of silica nanotubes at pH 9 over the investigated reaction time, the inner diameter obviously was reduced from 5.4 nm to 2.3 nm as the reaction time increased from 8 days to 16 days. Assuming here no simultaneous occurrence of peptide nanotube formation and silicification as suggested by Pouget et al.,[33] this result indicates that some silica precursors got inside and resulted in inner silica precipitation. This is broadly consistent with the increased attraction between negatively charged silica intermediates and the positive charged template surface with increasing pH. This increased attraction is sufficient to allow negatively charged silica species to overcome the diffusing constraint and therefore diffuse into the inner surface.

When there is only silica nucleation along the outer surface of the peptide nanotubes, the resulting silica nanotubes are expected to have an inner diameter equal to the outer diameter of the template. However, this is not the case. The inner diameter became smaller (~6 nm) for the silica nanotubes formed at pH 7 and pH 9 (aged for 4 and 8 days), as shown in Figure 8. Both Meegan's observations and our observations have indicated that the calcination process had little influence on the internal diameters of the resulting silica nanotubes.[34,36] The reduction most likely results from the penetration of silicon species into the peptide layer during the biomineralization process. This phenomenon has also been observed during the silica nanotube formation on peptide nanofiber template by Yuwono et al.[35] The penetration allowed silica growth inward. Furthermore, as a result of the same penetration process, the silica deposited along the inner surface of the peptide nanotubes apparently grew outward. The combination of outward and inward growth made the middle cavity of the double-walled silica tubes invisible.

The mechanistic events are illustrated in Figure 10, taking due account of the mediation of silica nanotube formation by the self-assembled I_3K nanotubes. The surface of I_3K nanotubes is rich in lysine residues and therefore provides ample catalytic sites for the sol−gel reaction of TEOS. TEOS undergoes hydrolysis and condensation to form silicic acid and polysilicic acids. The silica intermediates are liable to deprotonation to produce negative charges, and the charged species are preferentially driven to the surface of I_3K nanotubes, leading to an enhanced local surface concentration of reactants. A silica shell then gradually forms around the peptide nanotubes initiated by charge neutralization and facilitated by further polycondensation of silanol and other negatively charged silica species. The thickness of the silica shell increases until the functional primary amine groups in the template surface are completely neutralized or embedded. Under neutral or acidic solutions, the interactions between peptide templates and silica species are relatively weak, because of the low degree of deprotonation of silanol groups, thus resulting in an observable degree of nontemplated precipitation. At pH 9, however, silica intermediates are highly negatively charged, so that they interact favorably with positively charged I_3K templates, resulting in the more exclusive formation of silica nanostructure inside and outside the peptide template. As the condensation of silica intermediates on the outer surface of the template reaches saturation, prolonging the aging time leads to the steady diffusion of negatively charged silica intermediates into the inner nanotube

dx.doi.org/10.1021/cm2003885 |*Chem. Mater.* 2011, 23, 2466–2474

and the subsequent deposition on the interior surface. In brief, the silicon species initially grow on the exterior surface of the template and this process will continue until a certain saturated thickness is reached. Precipitation on the interior surface will occur if the driving force is sufficiently large. Otherwise, silica deposition may occur rather randomly.

5. CONCLUSIONS

This work has reported a simple and easily controlled approach for synthesizing well-ordered silica nanotubes under ambient conditions. I_3K peptide nanotubes were used as templates, and no harsh chemicals or solution environments were required. Lysine residues present on the outer and interior surfaces of peptide nanotubes were responsible for catalyzing the sol−gel reaction of TEOS and the subsequent templating and structural direction. The self-assembly of silica was closely associated with the solution conditions: (1) increase in the ratio of TEOS to peptide increased the degree of nonspecific silica deposition, while decrease in the ratio favored the formation of well-ordered silica nanotubes; (2) an increase from pH 5 to pH 9 favored the templating effect, leading to well-ordered surface silica nucleation; (3) at pH 7, increases in reaction time increased the degree of nonspecific silica deposition, whereas, at pH 9, no nonspecific silica deposition occurred, even if the reaction was incubated for 16 days; (4) the templated nucleation occurred only on the outer surface of the peptide nanotubes at undersaturation at neutral pH (∼7) while silica could be further deposited on the interior surface of the peptide nanotubes when the reaction was undertaken at pH 9. These findings clearly indicate that, as the driving force between the negatively charged silica intermediates and the cationic template surfaces increased, silica intermediates could become easily deposited on the interior template surface. Through careful adjustment of these factors, morphological structure of silica nanotubes could be well-controlled.

■ ASSOCIATED CONTENT

Supporting Information. Figures showing the HPLC profile and MALDI-TOF mass spectrum of I_3K, and an SEM photograph of silica nanostructures obtained at basic pH. (PDF) This material is available free of charge via the Internet at http://pubs.acs.org.

■ AUTHOR INFORMATION

Corresponding Author

*Tel.: (+86)532-8698-1569 (H.X.), (+44)-161-306-3926 (J.R.L.). E-mail addresses: xuh@upc.edu.cn (H.X.), j.lu@manchester.ac.uk (J.R.L.).

■ ACKNOWLEDGMENT

We acknowledge critical reading of this manuscript by Professor Robert K. Thomas at Oxford University. This work was supported by the National Natural Science Foundation of China (Grant No. 21033005), the Natural Science Foundation of Shandong Province, China (Grant No. ZR2010BQ003), the Fundamental Research Funds for the Central Universities of China (Grant No. 10CX04022A), and the UK Physical Sciences and Engineering Research Council (EPSRC).

■ REFERENCES

(1) Iler, R. K. *The Chemistry of Silica*; John Wiley & Sons: New York, 1979.
(2) Kageyama, K.; Tamazawa, J.; Aida, T. *Science* **1999**, *285*, 2113.
(3) Luckarift, H. R.; Spain, J. C.; Naik, R. R.; Stone, M. O. *Nat. Biotechnol.* **2004**, *22*, 211.
(4) Slowing, I. I.; Trewyn, B. G.; Giri, S.; Lin, V. S.-Y. *Adv. Funct. Mater.* **2007**, *17*, 1225.
(5) Hartmann, M. *Chem. Mater.* **2005**, *17*, 4577.
(6) Stöber, W.; Fink, A.; Bohn, E. *J. Colloid Interface Sci.* **1968**, *26*, 62.
(7) Morse, D. E. *Trends Biotechnol.* **1999**, *17*, 230.
(8) Patwardhan, S V.; Maheshwari, R.; Mukherjee, N.; Klick, K. L.; Clarson, S. J. *Biomacromolecules* **2006**, *7*, 491.
(9) Aizenberg, J.; Weaver, J. C.; Thanawala, M. S.; Sundar, V. C.; Morse, D. E.; Fratzl, P. *Science* **2005**, *309*, 275.
(10) Sundar, V. C.; Yablon, A. D.; Grazul, J. L.; Ilan, M.; Aizenberg, J. *Nature* **2003**, *424*, 899.
(11) Hamm, C. E.; Merkel, R.; Springer, O.; Jurkojc, P.; Maier, C.; Prechtel, K.; Smetacek, V. *Nature* **2003**, *421*, 841.
(12) Sumper, M.; Kröger, N. *J. Mater. Chem.* **2004**, *14*, 2059.
(13) Sumper, M.; Brunner, E. *Adv. Funct. Mater.* **2006**, *16*, 17.
(14) Dickerson, M. B.; Sandhage, K. H.; Naik, R. R. *Chem. Rev.* **2008**, *108*, 4935.
(15) Patwardhan, S. V.; Clarson, S. J.; Perry, C. C. *Chem. Commun.* **2005**, 1113.
(16) Halas, N. J. *ACS Nano* **2008**, *2*, 179.
(17) Shimizu, K.; Cha, J.; Stucky, G. D.; Morse, D. E. *Proc. Natl. Acad. Sci. U.S.A.* **1998**, *95*, 6234.
(18) Cha, J. N.; Shimizu, K.; Zhou, Y.; Christiansen, S. C.; Chmelka, B. F.; Stucky, G. D.; Morse, D. E. *Proc. Natl. Acad. Sci. U.S.A.* **1999**, *96*, 361.
(19) Kröger, N.; Deutzmann, R.; Sumper, M. *Science* **1999**, *286*, 1129.
(20) Kröger, N.; Deutzmann, R.; Sumper, M. *J. Biol. Chem.* **2001**, *276*, 26066.
(21) Tacke, R. *Angew. Chem., Int. Ed.* **1999**, *38*, 3015.
(22) Patwardhan, S. V.; Mukherjee, N.; Steinitz-Kannan, M.; Clarson, S. J. *Chem. Commun.* **2003**, 1122.
(23) Noll, F.; Sumper, M.; Hampp, N. *Nano Lett.* **2002**, *2*, 91.
(24) Belton, D. J.; Patwardhan, S. V.; Perry, C. C. *J. Mater. Chem.* **2005**, *15*, 4629.
(25) Delak, K. M.; Sahai, N. *Chem. Mater.* **2005**, *17*, 3221.
(26) Sumper, M. *Angew. Chem., Int. Ed.* **2004**, *43*, 2251.
(27) Yuan, J.-J.; Jin, R.-H. *Adv. Mater.* **2005**, *17*, 885.
(28) Tomczak, M. M.; Glawe, D. D.; Drummy, L. F.; Lawrence, C. G.; Stone, M. O.; Perry, C. C.; Pochan, D. J.; Deming, T. J.; Naik, R. R. *J. Am. Chem. Soc.* **2005**, *127*, 12577.
(29) Patwardhan, S. V.; Clarson, S. J. *J. Inorg. Organomet. Polym.* **2003**, *13*, 49.
(30) Cha, J. N.; Stucky, G. D.; Morse, D. E.; Deming, T. J. *Nature* **2000**, *403*, 289.
(31) Jan, J. -S.; Lee, S.; Carr, C. S.; Shantz, D. F. *Chem. Mater.* **2005**, *17*, 4310.
(32) Holmström, S. C.; King, P. J. S.; Ryadnov, M. G.; Butler, M. F.; Mann, S.; Woolfson, D. N. *Langmuir* **2008**, *24*, 11778.
(33) Pouget, E.; Dujardin, E.; Cavalier, A.; Moreac, A.; Valëry, C.; Marchi-Artzner, V.; Weiss, T.; Renault, A.; Paternostre, M.; Artzner, F. *Nat. Mater.* **2007**, *6*, 434.
(34) Meegan, J. E.; Aggeli, A.; Boden, N.; Brydson, R.; Brown, A. P.; Carrick, L.; Brough, A. R.; Hussain, A.; Ansell, R. J. *Adv. Funct. Mater.* **2004**, *14*, 31.
(35) Yuwono, V. M.; Hartgerink, J. D. *Langmuir* **2007**, *23*, 5033.
(36) Xu, H.; Wang, Y.; Ge, X.; Han, S.; Wang, S.; Zhou, P.; Shan, H.; Zhao, X.; Lu, J. R. *Chem. Mater.* **2010**, *22*, 5165.
(37) Xu, H.; Wang, J.; Han, S.; Wang, J.; Yu, D.; Zhang, H.; Xia, D.; Zhao, X. *Langmuir* **2009**, *25*, 4115.
(38) Zhao, X. B.; Pan, F.; Xu, H.; Yaseen, M.; Shan, H.; Hauser, C. A. E.; Zhang, S.; Lu, J. R. *Chem. Soc. Rev.* **2010**, *39*, 3480.

(39) Pan, F.; Zhao, X. B.; Perumal, S.; Waigh, T. A.; Lu, J. R.; Webster, J. R. P. *Langmuir* **2010**, *26*, 5690.
(40) Wang, J.; Han, S.; Meng, G.; Xu, H.; Xia, D.; Zhao, X. B.; Schweins, R.; Lu, J. R. *Soft Matter* **2009**, *5*, 3870.
(41) Zhao, X. B.; Pan, F.; Perumal, S.; Xu, H.; Lu, J. R.; Webster, J. R. P. *Soft Matter* **2009**, *5*, 1630.
(42) Lu, J. R.; Perumal, S.; Hopkinson, I.; Webster, J. R. P.; Penfold, J.; Hwang, W.; Zhang, S. *J. Am. Chem. Soc.* **2004**, *126*, 8940.
(43) Lu, J. R.; Perumal, S.; Powers, E. T.; Kelly, J. W.; Webster, J. R. P.; Penfold, J. *J. Am. Chem. Soc.* **2003**, *125*, 3751.
(44) Zhou, F.; Li, S.; Vo, C. D.; Yuan, J. J.; Chai, S.; Gao, Q.; Armes, S. P.; Lu, C.; Cheng, S. *Langmuir* **2007**, *23*, 9737.
(45) Hook, R. J. *J. Non-Cryst. Solids* **1996**, *195*, 1.
(46) Coradin, T.; Durupthy, O.; Livage, J. *Langmuir* **2002**, *18*, 2331.